

Bézier Base Extended Isogeometric Numerical Method for Thermo Elastic-Plastic Analysis of Crack Propagation in Cracked Plate under Welding Residual Stress and Thermal Load

Mohammad M. Shoheib^a, Shahram Shahrooi^a,
Mohammad Shishehsaz^{a,b} and Mahdi Hamzehei^a

^a*Department of Mechanical Engineering, Ahvaz Branch, Islamic Azad University, Ahvaz, Iran*

^b*Department of Mechanical Engineering, Faculty of Engineering, Shahid Chamran University of Ahvaz, Ahvaz, Iran*

E-mail(*corresp.*): shahramshahrooi@iauahvaz.ac.ir

Received August 24, 2021; revised October 9, 2022; accepted October 13, 2022

Abstract. A new procedure in the field of Bézier base extended isogeometric method (XIGA) has been introduced to analyze the effect of welding residual stress and thermal load on crack propagation rate and fatigue life. This new procedure is based on the constitutive thermoelastic plastic equation. The main parts of this procedure are using the Bézier base XIGA method to calculate the redistribution of welding residual stress due to crack growth and to compute the value of stress intensity factor (SIF) in the welding residual stress field. For this purpose, the grid points of Bézier elements (with C^0 -continuity) around the crack line and the crack tip are identified by the level set representation. Then, discontinuous enrichment functions are added to the isogeometric analysis approximation. Thus, this method does not require the re-meshing process. The results show that there is a good agreement between the results of proposed numerical method and the Hole-Drilling Strain-Gage method. The interaction integral method has been used to extract SIF. The effects of welding residual stress and thermal load on the SIF are considered using the superposition method. Also, the Walker equation has been modified to calculate the fatigue life caused by thermal loading and welding residual stress. The results display a good agreement between the proposed method and the finite element method. Due to the advantages of the Bézier based XIGA method, which eliminates parametric space and allows the precise addition of enrichment functions to the basis functions of cracked elements (crack line or crack tip), the obtained results are highly accurate that shows this method is effective for analyzing discontinuous problems.

Keywords: isogeometric method, Bézier extraction operator, Welding residual stress, stress intensity factor, fatigue life.

AMS Subject Classification: 65M12; 65M50; 70-08; 74S30; 74R99; 80M25.

1 Introduction

The most important effect of welding on mechanical parts is residual stress. Crack and defects caused by residual stress are the common defects in mechanical parts. Welding is a reliable and effective joining process in metals. The presence of residual stresses can be detrimental to the performance of the welded product. The butt-weld is a common type of welding joint. The residual stress can be harmful to the welded part performance. Tensile residual stresses generally increasing the susceptibility of a weld to stress cracking, fracture and fatigue [23]. In defects growth assessing the welding residual stress may give a large quota in total stress field than stress caused by mechanical loads [5]. Welding residual stress may result in some failure mechanisms such as brittle fracture and fatigue. Therefore, in the presence of mechanical load and residual stress in welded parts, the probability of failure due to fatigue is greatly increased and it is very important to investigate this cases. Numerical methods have been widely used in various sciences [19, 28, 29, 42]. These methods have high accuracy and acceptable convergence rate [8, 18, 34]. Thus, numerical methods have been presented to find an accelerate and possible solution in this case. The finite element method (FEM) has been widely used to obtain the residual stress caused by the welding [34, 42], and also to compute the SIF of crack [33]. In terms of crack growth problems and thermoelastic plastic analysis, FEM analysis has some weak points such as being time-consuming in SIF calculation. To overcome these weak points, new numerical methods have been introduced like the meshfree method and isogeometric method (IGA).

In the meshfree method, known as the meshless method there is no mesh in the domain of the problem [32]. Isogeometric analysis numerical method has been performed successfully [13, 15, 38] in some numerical methods such as FEM. The fundamental concept of isogeometric method is that the analysis receives geometry data directly from computer-aided design (CAD) models and uses a geometric basis function, as used in CAD, within the modeling and analysis process. Fundamental basis function in CAD is B-spline or NURBS. In comparison with Lagrange and Hermit basis functions that are used in finite element method, this kind of basis function can achieve higher continuity of derivatives. The Bézier extraction operator approach can be used with the isogeometric analysis. By choosing Bernstein functions as basis functions, an isogeometric analysis similar to that performed on the traditional finite element will be performed. Bernstein functions have a C^0 -continuity similar to Lagrange functions. The Bézier extraction operator allows the NURBS based isogeometric analysis numerical method to be incorporated into the traditional finite element method framework.

The isogeometric numerical method is used in numerous fields. Nguyen et al. [24] employed isogeometric Bézier FEM with a C^0 -type shear deforma-

tion theory for structural vibration analysis of functionally graded piezoelectric porous plates. They showed that the results of this method are very consistent with similar numerical studies or other solutions in the literature. Kumar et al. [31] studied the stress intensity factor on the crack tip plastic zones by XIGA. This study showed the effect of holes on the extent of crack tip plastic zones. Shuohui et al. [40] developed a novel method for the analysis of static and dynamic crack problems in elastic solids by XIGA analysis. Their proposed method provides several advantages in fracture modeling and analysis. Tran et al. [36] employed IGA for the buckling, static and dynamic response of plates. Huang et al. [12] performed analytical characterizations of the crack tip stress field and crack tip plastic zone for central cracked unstiffened and stiffened plates under biaxial loading. Yuan et al. [41] studied mode-I stress intensity factor for cracked special-shaped shells under bending load. Nguyen et al. [26] employed XIGA to analyze through-thickness cracks in thin shell structures. Bhardwaj et al. [3] performed fatigue crack life analysis in functionally graded material using XIGA. Also, continuous research has been done on the combination of meshfree and XIGA methods (adaptive isogeometric-meshfree coupling approach) [11, 20, 25] and also XIGA methods and FEM method [14, 16, 17] to investigate different parameters in cracked structures. This research was done in order to take advantage of both methods, which also had acceptable and important results.

In this study, the extended IGA is employed to investigate the fatigue life of a plate with welding residual stress and thermal load. A new formulation is presented to calculate the temperature distribution and residual stresses in a welding process. The stress field is then analyzed in the presence of crack and crack growth. In addition, the temperature and stress fields caused by thermal loading are calculated in the presence of crack. To validate the IGA results of residual stresses, the results of the hole-drilling strain-gauge method were used. To avoid re-meshing process, the grid points around the crack line and the crack tip are identified by representing the level set, and discontinuous enrichment functions are added to the isogeometric analysis approximation. The interaction integral method is used to extract SIF. The superposition principle is used to investigate the effect of welding residual stress and thermal loading on the effective SIF. The Walker equation is modified to calculate the fatigue life caused by thermal loading and residual stress due to welding. To confirm the results, FEM analysis was done under the same conditions. Prediction of fatigue life with the proposed procedure showed a good agreement with FEM results.

2 Constitutive equations for thermo elastic-plastic stress

The governing equation for the 2D problem in the domain Ω and the boundary Γ is explained as

$$\sigma_{ij,j} + b_i = 0,$$

where $i, j = (1, 2)$ denote the x and y coordinates, respectively and b is the external traction.

The initial and boundary conditions are as follows:

$$\sigma_{ij}n_j = \bar{t}_i \quad \text{on } \Gamma_t \quad \text{and} \quad u_i = \bar{u}_i \quad \text{on } \Gamma_u,$$

where \bar{u}_i and \bar{t}_i represent the displacement and tractions, respectively, and n_j is the component of the unit vector that is normal to the boundary. Because of the high rate of temperature rise in the welding and low yield stress at high temperatures, plastic strain is produced in the material. Therefore, to analyze the behavior of materials and calculate the welding residual stress, the use of thermoelastic plastic equations is necessary.

$$[d\sigma] = [D^{ep}]\{d\epsilon\} - [D^{th}]dT \quad \text{and} \quad [D^{ep}] = [D^e] - [D^p],$$

where $[D^{ep}]$ is the elastic-plastic stiffness matrix, $[D^e]$ and $[D^p]$ are the elastic and plastic stiffness matrix, respectively, and $[D^{th}]$ is the thermal stiffness matrix.

Due to the nonlinear dependence between strains and stresses in the material, the material stiffness cannot be considered constant. Equations that describe the appropriate dependency are defined in a variety of methods. In this study, the incremental plasticity method has been used to define the constitutive equations, which describes the appropriate dependence. The material is modeled with thermoelastic plastic behavior and temperature-dependent properties. Also, plasticity is independent of rate and is modeled using the kinematic hardening, associated flow rule and von Mises criterion.

Thus, using the plasticity theory, the thermoelastic plastic equation is defined as [37]

$$\begin{aligned} \{d\sigma\} = & [D^{ep}]\{e\epsilon\} - [D^{ep}] \left(\{a\}dT + \frac{\partial[D^e]^{-1}}{\partial T}\{\sigma\}dT + \frac{\partial[D^e]^{-1}}{\partial \bar{\epsilon}}\{\epsilon\}d\bar{\epsilon} \right) \\ & - \frac{[D^e]\{\sigma\}}{S} \left(\frac{\partial F}{\partial T}dT + \frac{\partial F}{\partial \bar{\epsilon}}d\bar{\epsilon} \right), \end{aligned}$$

where $\{a\}$ is the linear thermal expansion coefficient matrix, $\bar{\epsilon}$ is the rate of strain, σ is the effective stress and F is the yield function.

3 Isogeometric analysis numerical method

3.1 NURBS basis functions

The B-spline basis functions are basic concepts of the IGA method, that can be defined using a knot values wick called knot vector, $\Xi = \{\xi_1, \xi_2, \dots, \xi_{n+p+1}\}$ ($\xi \in R$), where n is the number of the basis functions and p is the order of the polynomial. The *B - spline* functions define as [2]

$$N_{i,0} = \begin{cases} 1, & \xi_i \leq \xi < \xi_{i+1} \\ 0, & \text{otherwise,} \end{cases} \quad \text{for } p = 0,$$

and

$$N_{i,p}(\xi) = \frac{\xi - \xi_i}{\xi_{i+p-1} - \xi_i} N_{i,p-1}(\xi) + \frac{\xi_{i+p} - \xi}{\xi_{i+p} - \xi_{i+1}} N_{i+1,p-1}(\xi) \quad \text{for } p > 0.$$

The NURBS surfaces are defined as

$$S(\xi, \eta) = \sum_{i=1}^n \sum_{j=1}^m R_{i,p}(\xi, \eta) P_{i,j},$$

where $P_{i,j}$ forms an $n \times m$ set of control points and $R(\xi, \eta)$ represents NURBS basis function defined as

$$R(\xi, \eta) = \frac{N_{i,p}(\xi)M_{j,q}(\eta)w_{i,j}}{\sum_{i=0}^n \sum_{j=0}^m N_{i,p}(\xi)M_{j,q}(\eta)w_{i,j}},$$

where $w_{i,j,k}$ represents the weights corresponding to the control point.

3.2 Bézier extraction of NURBS

The traditional spans of Bézier element are $[0, 1]$ (in each direction) created by a knot vector without the internal value. This knot vector contains $(p+1)$ zeros and ones, where p is the order of the polynomial. The basis functions created by this kind of knot vector are named the Bernstein functions and have many similarities to the Lagrange basis functions that are used in the finite element method. The Bernstein functions can be defined as [27]

$$B_{i,p}(\xi) = (1 - \xi)B_{i,p-1}(\xi) + \xi B_{i-1,p-1}(\xi),$$

$$B_{0,p}(0) = B_{p,p}(1) = 1, \quad B_{i,p}(\xi) = 0 \quad \text{if } i < 0, i > p.$$

These Bernstein functions, similar to the $B - splines$ and NURBS functions, constitute the partition of unity and are nonnegative over the entire domain. In addition, the Bernstein functions identical to the Lagrange functions are symmetric and interpolator at the endpoints of the domain.

The i^{th} derivatives of Bernstein functions are defined in Equation (3.1):

$$\frac{B_{i,p}(\xi)}{d\xi} = p [B_{i-1,p-1}(\xi) - B_{i,p-1}(\xi)] \quad B_{-1,p-1}(\xi) = B_{p,p-1}(\xi) = 0. \quad (3.1)$$

Similar to the $B - spline$ and NURBS curve, a Bézier curve can be evaluated by a linear combination of Bernstein functions and the set of control point coordinates as

$$C(\xi) = \sum_{i=0}^p B_i^p(\xi) P_i = P^T B(\xi).$$

The Bézier extraction operator maps linear combinations of Bernstein functions (Bézier basis functions) into NURBS basis functions. So, it is possible to use piecewise C^0 -continuous Bézier elements in IGA analysis similar to FEM. To decompose NURBS basis functions to Bézier elements (Bézier decomposition) all internal values of the knot vector must be repeated until multiplicity becomes equal to p . The Bézier extraction operator defined using the equations between the new control points and the original control points when a knot is

repeated. Assuming that $\bar{\xi} \in [\xi_k, \xi_{k+1}]$ ($k > p$) is a new knot that inserts into the existing knot vector $\Xi = \{\xi_1, \xi_2, \dots, \xi_{n+p+1}\}$, a new set of control points can be created as [6]

$$\bar{P}_i = \begin{cases} P_1, & i = 1, \\ \alpha_i P_i + (1 - \alpha_i) P_{i-1}, & 1 < i < m, m = n + 1, \\ P_n, & i = m, \end{cases} \tag{3.2}$$

$$\alpha_i = \begin{cases} 1, & i \leq K - P, \\ \frac{\bar{\xi} - \xi_k}{\xi_{i+p} - \xi_i}, & K - P + 1 \leq i \leq K, \\ 0, & i \geq K + 1, \end{cases}$$

where \bar{P} and P_{ii} are the new and the existing control points, respectively. Based on the operation of knots insertion, given a new set of knots $\{\bar{\xi}_1, \bar{\xi}_2, \dots, \bar{\xi}_m\}$, the Bézier extraction operator C_j ($j = 1, 2, \dots, m$) can be determined in a matrix form as

$$C_j = \begin{bmatrix} \alpha_1 & 1 - \alpha_2 & 0 & & 0 \\ 0 & \alpha_2 & 1 - \alpha_3 & \dots & 0 \\ 0 & 0 & \alpha_3 & & 0 \\ & & \vdots & \ddots & \vdots \\ 0 & 0 & 0 & \dots & \alpha_{(n+j-1)}(1 - \alpha_{(n+1)}) \end{bmatrix}.$$

Consequently, Equation (3.2) can be recast in a matrix form to present the sequence of control points created by the knot insertion operation.

$$\bar{P}_{i+1} = (C_j)^T \bar{P}_j, \quad \text{where } \bar{P}_1 = P.$$

The final control points $\bar{P}_{m+1} = P_b$ are explained as:

$$C^T = (C_m)^T (C_{m-1})^T \dots (C_1)^T.$$

The equation between the original NURBS control points and the new Bézier control points is defined as $\bar{P} = C^T P$. Given that the insertion of a node does not change the parametric or geometric nature of the curve, so it can be written,

$$C(\xi) = (\bar{P})^T B(\xi) = (C^T P)^T B(\xi) = P^T C B(\xi) = P^T N(\xi),$$

therefore, the equation between the B-spline basis functions and the Bernstein functions defined as $N(\xi) = C B(\xi)$, where, C is called the Bézier extraction operator. The surfaces created by the NURBS basis functions and the Bézier basis functions are entirely similar

The bivariate Bézier extraction operator is defined as $C_A^e = C_\xi^i \otimes C_\eta^j$.

4 Thermal and residual stress analysis in welding process

To calculate the welding-residual stress distribution, the temperature distribution due to welding must first be calculated. For thermal analysis of the part

during welding it can be considered as a finite volume with the surface S . The heat transfer equation for the mentioned boundary volume explained as

$$-\nabla \cdot \vec{q}(x, y, z, t) + Q(x, y, z, t) = \rho C \frac{\partial T(x, y, z, t)}{\partial t}, \tag{4.1}$$

where \vec{q} is the heat flux vector, Q is the generated heat by the internal heat source, ρ is the density, C is the special heat capacity and T is the temperature at any moment. The Fourier law for heat flux is as follows:

$$\vec{q} = k \nabla T, \tag{4.2}$$

where k is the heat conductivity coefficient. By combining Equation (4.1) and Equation (4.2), the following equation is obtained,

$$\rho C \frac{\partial T}{\partial t} = Q + \left[\frac{\partial}{\partial x} \left(K_x \frac{\partial T}{\partial x} \right) + \frac{\partial}{\partial y} \left(K_y \frac{\partial T}{\partial y} \right) + \frac{\partial}{\partial z} \left(K_z \frac{\partial T}{\partial z} \right) \right]. \tag{4.3}$$

If the part is in contact with a fluid and there is a temperature difference between them, there will also be convection heat transfer and Equation (4.3) will be written as follows:

$$\rho C \frac{\partial T}{\partial t} + \frac{hP}{A} (T - T_\infty) = Q + \left[\frac{\partial}{\partial x} \left(K_x \frac{\partial T}{\partial x} \right) + \frac{\partial}{\partial y} \left(K_y \frac{\partial T}{\partial y} \right) + \frac{\partial}{\partial z} \left(K_z \frac{\partial T}{\partial z} \right) \right],$$

where P is the perimeter of area A and h is the heat convection coefficient. This equation is a nonlinear equation and is solved using initial and boundary conditions. The temperature-dependent physical properties of the material are also required.

In order to achieve the element weak form differential equation of thermal problems instead of minimizing potential energy function, a similar function will be minimized and the same force vector and stiffness matrix will be obtained.

$$\mathbf{K}\mathbf{T}(t) + \mathbf{m}\dot{\mathbf{T}}(t) = \mathbf{f}(t), \quad \mathbf{f}(t) = \mathbf{f}_Q + \mathbf{f}_q + \mathbf{f}_h, \tag{4.4}$$

where

$$\mathbf{k} = \int \mathbf{B}^T \mathbf{D}^{th} \mathbf{B} d\Omega + \int h \mathbf{R}^T \mathbf{R} dS, \quad \mathbf{m} = \int C \rho \mathbf{R}^T \mathbf{R} d\Omega,$$

$$\mathbf{f}_Q = \int \mathbf{R}^T \mathbf{Q} d\Omega, \quad \mathbf{f}_q = \int \mathbf{R}^T \mathbf{q} dS, \quad \mathbf{f}_h = \int \mathbf{R}^T h T_\infty dS.$$

Using the backward difference technique to approximate time, for each time step, Equation (4.4) written as:

$$\left(m + \frac{1}{2} k \Delta t \right) T_{n+1} = f \Delta t + \left(m - \frac{1}{2} k \Delta t \right) T_n.$$

The initial (thermal) strain can be calculated as follows:

$$\left\{ \begin{matrix} \varepsilon_{11}^{th} \\ \varepsilon_{22}^{th} \\ 2\varepsilon_{12}^{th} \end{matrix} \right\} = \left\{ \begin{matrix} \alpha_{11} \\ \alpha_{22} \\ 0 \end{matrix} \right\} \Delta T,$$

where \aleph_{ij} and ΔT denote the thermal expansion coefficient and temperature gradient, respectively.

After obtaining the temperature field of welding, this temperature field is applied as a loading and the welding residual stress is calculated from the mechanical analysis. The force vectors and stiffness matrix will be obtained as

$$\mathbf{k}\mathbf{u} = \mathbf{P} + \mathbf{F} + \mathbf{R},$$

where K (the local elastic-plastic stiffness matrix) and thermomechanical load vectors are obtained as:

$$\mathbf{k} = \int_{\Omega_q} \mathbf{V}_I^T \mathbf{D}^{ep} \mathbf{B} d\mathbf{u} d\Omega - \int_{\Gamma_{qu}} \mathbf{W}_I^T n \mathbf{D}^{ep} \mathbf{B} d\mathbf{u} d\Gamma,$$

$$\mathbf{P} = \int_{\Omega_q} \mathbf{V}_I^T \mathbf{D}^{th} dT d\Omega \ \& \ \mathbf{F} = \int_{\Gamma_{qt}} \mathbf{W}_I (\bar{\mathbf{t}}_i + d\bar{\mathbf{t}}_i) d\Gamma \ \& \ \mathbf{R} = \int_{\Omega_Q} \mathbf{V}_I^T \boldsymbol{\sigma} d\Omega.$$

5 Extended isogeometric analysis

5.1 Level set technique

The level set technique is used in the cracked models to identify the crack line and crack tip, in which a crack is defined by two orthogonal level set fields [30]. The first field defines the crack line $\{x: \phi(x)=0 \text{ and } \psi(x) \leq 0\}$, and other one defines the crack tip $\{x: \varphi(x)=0 \text{ and } \psi(x)=0\}$. The local enrichment function is then used to describe crack geometry independently of the mesh without the need for a re-meshing process for the crack growth analysis. This implicit definition of crack line and crack tip by the level set is illustrated in Figure 1.

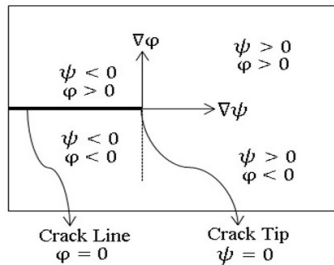


Figure 1. Crack line function φ and crack tip function Ψ .

In this technique, φ denotes the distance to the extended crack line, and ψ denotes the distance to the line that intercross the crack line at the crack tip and is perpendicular to the crack line.

In the given control point, the amount of φ is the minimum interval between the control points and the crack line. Considering that (x_0, y_0) and (x_1, y_1) represent the coordinates of the starting point and end point of a crack, and $p = (x, y)$ is a control point where the minimum interval is calculated, and n is the unit vector that is normal to the element that containing this control

point, φ is defined as:

$$\varphi = (x - y) \cdot n = \frac{(y_0 - y_1)x + (x_1 - x_0)y + (x_0y_1 - x_1y_0)}{\sqrt{(x_1 - x_0)^2 + (y_1 - y_0)^2}},$$

where φ is calculated for each control point to recognize the elements that are cut by the crack line. Also, the crack tip function, ψ , defined as:

$$\psi = ([xy] - [x_1y_1]) \cdot \left(\frac{(x_1 - x_0)\vec{l} + (y_1 - y_0)\vec{J}}{|(x_1 - x_0)\vec{l} + (y_1 - y_0)\vec{J}|} \right).$$

Similarly, the amount of ψ is the minimum distance between each control point and the crack tip. ψ is calculated for each control point of the model to recognize the element around the crack tip. On the other hand, $\max(\varphi) \times \min(\varphi) < 0$ and $\max(\psi) < 0$ is valid for the split knot span (element) and $\max(\varphi) \times \min(\varphi) < 0$ and $\max(\psi) \times \min(\psi) < 0$ is valid for the crack tip knot span (element).

5.2 XIGA approximations for crack problems

In the XIGA method, the approximation of displacement is locally enriched by asymptotic enrichment function to simulate discontinuities. For this purpose, several number of fictitious nodes (and their degrees of freedom) are added to the control points of the elements consisting of the crack line and the crack tip. The basic concept of XIGA is the extent of approximation of the basis functions by special enrichment functions selected according to the behavior of the crack problem. In the cracked model, the elements divided by the crack line and the crack tip are recognized as enriched elements.

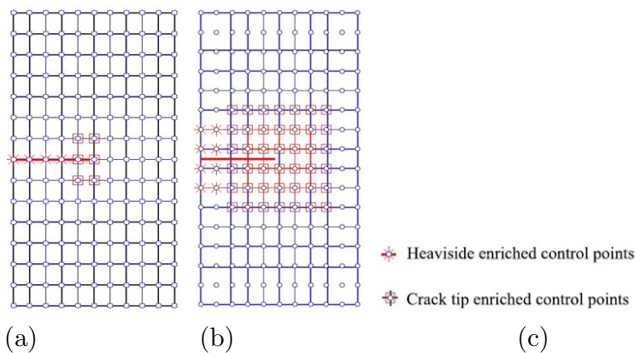


Figure 2. Crack geometry and enriched control points, (a) basis functions of order 1, (b) basis functions of order 3, (c) Heaviside enriched control points and crack tip enriched control points.

Furthermore, in XIGA, cracks independent of the meshing process are shown, and hence, re-meshing process is not required for the analysis of crack propagation. The level set technique is used to identify the enriched and non-enriched elements as well as their control points. The XIGA discretization with

the enriched control points is shown in Figure 2. The typical XIGA discretization with the enriched control points is shown in Figure 2(a), and Figure 2(b) for basis functions of orders 1 and 3, respectively.

The control points associated with the split elements are enriched with the Heaviside function whilst the control points associated with the tip elements are enriched with the crack tip enrichment functions. The XIGA approximations in the two-dimensional continuum formulation for cracks are given as [4, 35]

$$u(\xi) = \sum_{i=1}^{n_{el}} \mathbf{R}_i(\xi) \mathbf{u}_i + \sum_{j=1}^{n_h} \mathbf{R}_i(\xi) [H(\xi) - H(\xi_i)] \mathbf{a}_j + \sum_{k=1}^{n_t} \mathbf{R}_k(\xi) \left\{ \sum_{\alpha=1}^4 [Q_\alpha(\xi) - Q_\alpha(\xi_i)] \mathbf{b}_k^\alpha \right\}. \quad (5.1)$$

The first term in Equation (5.1) represents the standard isogeometric analysis approximation. Additionally, $R_i(\xi)$ is the basis function and u_i is the standard (without enrichment) degrees of freedom related to a special control point. Other terms in the displacement field are used to represent the discontinuous behavior by enrichment function. Where $H(\xi)$ s are the Heaviside functions and $Q_\alpha(\xi)$ s are the asymptotic enrichment functions for crack tip. Moreover, a_j and b_k^α are the additional degrees of freedom related to the modeling crack line and the crack tip, and n_t and n_h are the number of enriched control points with asymptotic enrichment functions of crack tip and Heaviside functions, respectively.

The $H(\xi)$ function is equal to +1 or -1 based on the location of the control point concerning the crack lines. For each individual control point, the $H(\xi)$ is equal to +1 if this control point lies above the crack line, otherwise it will be -1. The asymptotic enrichment functions of crack tip are defined as

$$Q_\alpha(\xi) = \left\{ \sqrt{r} \cos \frac{\theta}{2}, \sqrt{r} \sin \frac{\theta}{2}, \sqrt{r} \cos \frac{\theta}{2} \sin \theta, \sqrt{r} \sin \frac{\theta}{2} \sin \theta \right\}.$$

In these functions, r and θ are the polar coordinates of a point concerned with the crack tip.

Due to the fact that in the residual weighting method, the spline function is also used as a weight function, the same enrichment function has been used to enrich these functions. In fact, the basis function and the weight function in this method are considered the same as the basis function and the shape function in the isogeometric method. The discrete system of the following equations is obtained as

$$[k]\{a\} = \{F\},$$

where, $[K]$ is the global stiffness matrix, $\{a\}$ is the vector of nodal unknowns and $\{f\}$ is the vector of external force. The displacement control variables and the additional enrichment degrees of freedom are as follows:

$$\mathbf{U} = \{u \ a \ b_1 \ b_2 \ b_3 \ b_4\}^T.$$

The global stiffness matrix \mathbf{K} is explained as:

$$\mathbf{k}^e = \int (\mathbf{B}_i^r)^T \mathbf{D} \mathbf{B}_j^s d\Omega, \quad r, s = u, a, b.$$

The global force vector \mathbf{F} is expressed as:

$$\mathbf{F}_i = \{F_i^u F_i^a F_i^{b1} F_i^{b2} F_i^{b3} F_i^{b4}\}^T,$$

$$F_i^u = \int [\mathbf{B}_i^T \mathbf{D} \boldsymbol{\varepsilon}^0] d\Omega - \int [\mathbf{B}_i^T \boldsymbol{\sigma}^0] d\Omega + \int [\mathbf{R}_i^T \mathbf{b}] d\Omega + \int [\mathbf{R}_i^T \mathbf{s}] dS,$$

$$F_i^a = \int [\mathbf{B}_i^T \mathbf{D} \boldsymbol{\varepsilon}^0] d\Omega - \int [\mathbf{B}_i^T H \boldsymbol{\sigma}^0] d\Omega + \int [\mathbf{R}_i^T H \mathbf{b}] d\Omega + \int [\mathbf{R}_i^T H \mathbf{s}] dS,$$

$$F_i^b = \int [\mathbf{B}_i^T Q_\alpha \mathbf{D} \boldsymbol{\varepsilon}^0] d\Omega - \int [\mathbf{B}_i^T Q_\alpha \boldsymbol{\sigma}^0] d\Omega + \int [\mathbf{R}_i^T Q_\alpha \mathbf{b}] d\Omega + \int [\mathbf{R}_i^T Q_\alpha \mathbf{s}] dS.$$

6 Interaction integral method

The present interaction integral approach for computing SIF is a two-state integration method with superposition of auxiliary and actual fields. In this method, small kinematic strain is assumed and the material is limited to linear elastic and isotropic. The interaction integral (M -integral) equation is derived from the J -integral equation. The J -integral [7] is explained as

$$J = \lim_{\Gamma \rightarrow 0} \int_{\Gamma} (w \delta_{1j} - \sigma_{ij} u_{i,1}) n_j d\Gamma,$$

where w is the density of strain energy that defined as follows: $w = \int_0^{\varepsilon_{kl}} \sigma_{ij} d\varepsilon_{ij}$, and n_j is the outward vector that is normal to the contour Γ , as shown in Figure 3, where \bar{u} is the displacement and $\bar{\tau}$ is the traction.

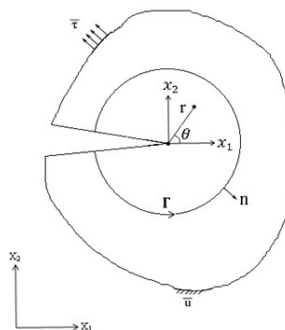


Figure 3. Coordinate systems and integration path.

If two supportable and independent fields are considered in a condition that the displacement, strain, and stress of the actual field and the auxiliary field

are denoted by (u, ε, σ) and $(u^{aux}, \varepsilon^{aux}, \sigma^{aux})$, respectively, then the J -integral of these fields defined as

$$J^s = \int_{\Gamma} \left\{ \frac{1}{2} (\sigma_{ik} + \sigma_{ik}^{aux}) (\varepsilon_{ik} + \varepsilon_{ik}^{aux}) \sigma_{1j} - (\sigma_{ij} + \sigma_{ij}^{aux}) (u_{i,1} + u_{i,1}^{aux}) \right\} n_j d\Gamma. \quad (6.1)$$

The integral Equation (6.1) is not the appropriate form for further evaluations. Thus, it is necessary to recast this integral into a similar domain form. This task would be done by multiplying the integrand by a sufficiently smooth weighting function q . This weighting function takes a value of unity on an open set including the crack front and losses on an outer prescribed contour. Based on this principle, \bar{M} can be defined as

$$\bar{M} = - \int_v \begin{pmatrix} u_{i,l} \sigma_{ij}^{aux} q_{l,j} + u_{i,l}^{aux} \sigma_{ij} a_{l,j} \\ -\sigma_{ij}^{aux} \varepsilon_{ij} q_{l,l} \end{pmatrix} dV + \int_v \begin{pmatrix} u_{i,l} \sigma_{ij}^{aux} + u_{i,l}^{aux} \sigma_{ij} \\ +u_{i,l}^{aux} f_i - \sigma_{ij,l}^{aux} \varepsilon_{ij} \end{pmatrix} q_q dV.$$

By superposing the actual and auxiliary fields the interaction integral $M(s)$ take the value as

$$M(S) = \frac{2}{E'} (K_I K_I^{aux} + K_{II} K_{II}^{aux}) + \frac{1}{\mu} K_{III} K_{III}^{aux},$$

where μ is the shear modulus and E' is defined using material parameters.

K_I is calculated by substituting the auxiliary field SIFs $K_I^{aux} = 1$ and $K_{II}^{aux} = K_{III}^{aux} = 0$ as [35]:

$$K_I = \frac{E'}{2} M(S) (K_I^{aux} = 1, K_{II}^{aux} = K_{III}^{aux} = 0).$$

7 Effective stress intensity factor

In the presence of residual stresses, the effective stress intensity factor is calculated based on the superposition principle. The effective stress intensity factor is mathematically explained as

$$k_{eff} = k_{ther} + k_{res},$$

where K_{ther} and K_{res} are the thermal SIF and residual stress SIF, respectively.

8 Fatigue crack growth

The cycle ratio is defined as $R = k_{min}/k_{max}$, where K_{max} and K_{min} are the minimum and maximum of SIF, respectively. When the cycle ratio is not zero, crack propagation is a function of both the cycle ratio changes and the SIF changes as follows:

$$\frac{da}{dN} = f(\Delta k, R).$$

The Walker equation is defined as [10]

$$\frac{da}{dN} = c(\overline{\Delta k})^m, \quad \overline{\Delta k} = k_{max}(1 - R)^\mu,$$

where μ is also dependent on the material properties.

In the presence of residual stress in the material, based on the superposition principle, the total SIF can be defined as follows:

$$\Delta k_{total} = \Delta k_{eff}^{max} - \Delta k_{eff}^{min} = (k_{ther}^{max} + k_{res}) - (k_{ther}^{min} + k_{res}) = \Delta k_{ther}.$$

Therefore, the Walker equation should be used, as defined below:

$$\frac{da}{dN} = c \{ (k_{max} - k_{min})(1 - R_{eff})^{\mu-1} \}^m,$$

where the effective cycle ratio is defined as

$$R_{eff} = (K_{ther}^{min} + k_{res}) / (K_{ther}^{max} + k_{res}).$$

Therefore, the Walker equation is modified based on R_{eff} as follows:

$$\frac{da}{dN} = c \left\{ (k_{max} - k_{min}) \left(\frac{\Delta k_{ther}}{k_{ther}^{max} + k_{res}} \right)^{\mu-1} \right\}^m. \tag{8.1}$$

9 Numerical results and discussion

9.1 Analysis conditions

The analyzed structure is a plate with a length and width of 300mm and a thickness of 2mm. The material of the plate is SUS304. The welding direction and the shape of the joint are schematically shown in Figure 4. Moreover, the thermal load and boundary conditions are specified in Table 1.

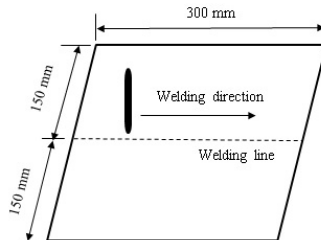


Figure 4. Dimension and welding details.

The gas tungsten arc welding process (GTAW) is used as the welding method. Welding time and heat input are considered $t = 90s$ and $Q = 110 \frac{J}{mm}$, respectively. In this study, the physical, mechanical and thermal properties of materials are temperature dependent [9].

9.2 Residual stress analysis by XIGA method

The analysis includes two steps. In first step, the temperature history of welding process is calculated. Then, in the second step, the temperature history is applied on the mechanical model to calculate the welding residual stress. The

Table 1. Dimensions and boundary condition of the plate.

Plate length	300 mm
Plate width	300 mm
Plate thickness	2 mm
Initial crack length	10 mm
Welding heat input	110 J/mm
Left edge(heat flux)	1000 KW/m ²
Right edge(constant)	300°C
Top edge	insulated
Bottom edge	insulated

mechanical solution is continued until all nodes reach ambient temperature. Also, due to the geometric symmetry and reduced computational cost, half of the model has been analyzed.

Thermal boundary condition is assumed for all plate boundaries. Also, radiation losses are considered for the weld zone, and convection losses are considered for parts far from the weld zone. In this study, the moving heat source is modeled and the same model and basis function are used in thermal and mechanical analysis. To display analysis result, several paths and points have been considered [22]. These paths are illustrated in Figure 5.

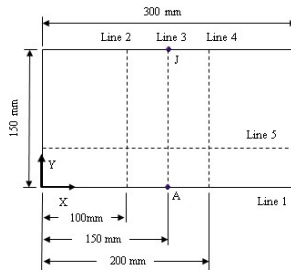


Figure 5. The considered path.

Also, the coordinates of the considered point are presented in Table 2.

Table 2. Coordinates of the considered point (mm).

Point	A	B	C	D	E	F	G	H	I	J
X	150	150	150	150	150	150	150	150	150	150
Y	0	5	10	20	25	30	60	90	120	150

The history of temperature at points A–J in the vertical direction on the welding line is presented in Figure 6 from the beginning of the welding process up to 300s later [22].

Table 3 shows the transverse and longitudinal welding residual stress along the lines 2, 3, 4 and the welding line. This table shows that in the direction

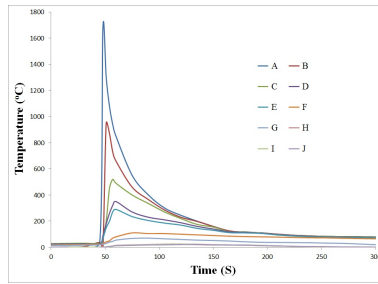


Figure 6. Temperature distribution on line 3 from 0 to 300s.

perpendicular to the welding line, the transverse residual stresses are significantly less than the longitudinal residual stresses. Also, the maximum value of welding residual tensile stress occurs in the line 2 and then reduces quickly to the residual compressive stress.

Table 3. Longitudinal and transverse residual stresses.

Welding line (line 1)			line 2			line 3			line 4		
X	Long.	Transv.	Y	Long.	Transv.	Y	Long.	Transv.	Y	Long.	Transv.
0	5.1	-200.3	0	251.7	35.3	0	245.7	31.6	0	239.3	30.7
20	150.4	-70.5	10	250.2	37.2	10	245.3	32.1	10	240.7	34.2
40	240.7	25.1	20	249.4	37.4	20	245.2	32.3	20	241.2	35.1
60	258.2	26.6	30	248.3	37.5	30	245.4	32.4	30	180.4	34.5
80	261.1	22.7	40	-100.1	35.8	40	-110.7	29.7	40	-130.3	30.5
100	259.3	20.4	50	-180.8	25.4	50	-146.2	24.6	50	-126.2	24.5
120	257.2	18.2	60	-125.5	15.3	60	-105.3	18.5	60	-92.5	17.2
140	255.3	16.5	70	-90.2	5.2	70	-78.5	14.5	70	-67.4	11.3
160	254.4	16.4	80	-65.1	0.4	80	-58.4	11.4	80	-48.9	7.6
180	255.6	18.6	90	-47.9	-2.9	90	-43.5	8.3	90	-35.7	4.5
200	257.7	21.4	100	-30.5	-3.5	100	-30.2	5.8	100	-24.2	2.4
220	257.4	23.8	110	-17.4	-2.7	110	-20.1	3.8	110	-17.3	1.5
240	253.9	27.2	120	-8.6	-2.0	120	-12.6	2.1	120	-12.5	0.9
260	230.8	26.9	130	-2.1	-1.1	130	-6.9	1.2	130	-6.3	0.5
280	105.2	-40.8	140	0.3	-0.5	140	-4.7	0.5	140	-4.1	0.2
300	2.7	-210.2	150	4.1	0	150	-1.2	0.1	150	-0.9	0

The Hole-Drilling method determines residual stresses based on the measured strains [1]. Table 4 shows the longitudinal and the transverse welding residual stresses along the lines 3 calculated by the IGA method and the Hole-Drilling method. This figure shows that the residual stresses results calculated by the presented method are obtained with acceptable accuracy.

9.3 Crack propagation in the residual stress field

Redistribution of the welding residual stress and strain during crack propagation was calculated by the XIGA method. Welding residual strain and stress were calculated for different crack lengths from 10mm to 25mm. Table 5 and

Table 4. Comparison of the results of residual stress distribution by Hole-Drilling method and IGA method.

Distance from Weld Line (mm)	Longitudinal (MPa)		Error (%)	Transverse(MPa)		Error (%)
	IGA	Hole Drilling		IGA	Hole Drilling	
0	245.7	252.1	2.54	31.6	29.9	5.69
10	245.3	249.7	2.51	32.1	31.2	2.89
20	245.2	248.2	1.21	32.3	31.8	1.57
30	245.4	246.9	0.61	32.4	31.7	2.21
40	-110.7	-113.2	2.21	29.7	30.4	2.31
50	-146.2	-147.5	0.89	24.6	25.7	4.28
60	-105.3	-103.4	1.84	18.5	17.9	3.35
70	-78.5	-77.1	1.82	14.5	13.7	5.84
80	-58.4	-60.2	2.91	11.4	10.6	7.53
90	-43.5	-45.1	3.73	8.3	7.9	7.61
100	-30.2	-31.4	3.82	5.8	5.3	9.43
110	-20.1	-20.9	3.83	3.8	4.1	7.31
120	-12.6	-13.1	3.78	2.1	2.3	8.69
130	-6.9	-6.7	2.98	1.2	1.4	14.28
140	-4.7	-4.5	4.45	0.5	0.6	16.67
150	-1.2	-1.1	9.10	0.1	0.122	18.01

Figure 7 show the redistribution of transverse and longitudinal welding residual strain and residual stresses for various crack lengths during crack propagation. Crack growth induced considerable change in longitudinal residual stress relative to transverse residual stress. Also, K_{res} for each crack length can be calculated from the stress redistribution in the same crack length according to the interaction integral method.

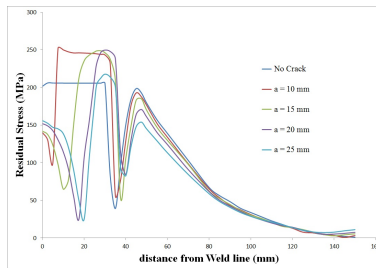


Figure 7. Von Mises stress for different crack lengths.

9.4 Stress field of thermal load around the crack

The temperature and stress distributions of thermal load in the welded plate were calculated by XIGA method. The stress redistribution in the x and y directions due to crack growth is presented in Figures 8 and 9, respectively. These figures show the stress distribution perpendicular to the weld line for different crack lengths along $y = 0$ to $y = 150$ mm as a function of distance from the weld line. There are considerable change in the stress field around the crack due to crack growth.

Table 5. Longitudinal and transverse strain for different crack lengths.

Distance	No Crack		a= 10 mm		a= 15 mm		a= 20 mm	
	Longit.	Transv.	Longit.	Transv.	Longit.	Transv.	Longit.	Transv.
0	0.00115	-0.0002	0.00018	-0.00071	0.0002	-0.00071	0.0001	-0.0076
10	0.001184	-0.0002	0.00134	0	0.000035	-0.0005	0.00009	-0.00069
20	0.0011801	-0.00019	0.00129	0	0.00129	0.0001	0.001281	0
30	-0.00004	0	0.00045	0.0001	0.00125	0.00016	0.00128	0.00025
40	-0.00082	0.00035	-0.00077	0.00041	-0.00069	0.00045	-0.00057	0.00049
50	-0.000665	0.00036	-0.00061	0.00039	-0.00054	0.00043	-0.00048	0.00046
60	-0.00048	0.00028	-0.00044	0.00031	-0.0004	0.00034	-0.00035	0.00036
70	-0.00035	0.00022	-0.00032	0.00024	-0.00029	0.00026	-0.00026	0.00028
80	-0.00026	0.00016	-0.00024	0.00018	-0.00022	0.0002	-0.0002	0.00021
90	-0.0002	0.000115	-0.00019	0.00013	-0.00017	0.000145	-0.00015	0.000155
100	-0.00016	0.00008	-0.00015	0.000095	-0.00013	0.00011	-0.00012	0.000115
110	-0.000122	0.000055	-0.00011	0.000067	-0.00011	0.000075	-0.0001	0.000085
120	-0.0001	0.000037	-0.00005	0.00005	-0.00009	0.00005	-0.00009	0.000055
130	-0.00008	0.000021	-0.00008	0.000022	-0.000075	0.000025	-0.000075	0.00003
140	-0.000066	0.00001	-0.00007	0.00001	-0.00007	0.00001	-0.00007	0.000012
150	-0.00006	0.000005	-0.00006	0.000005	-0.000055	0.000005	-0.000071	0.000004

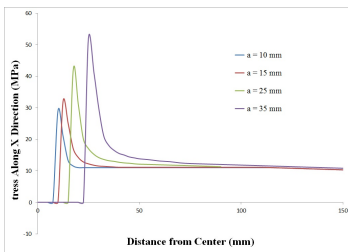


Figure 8. Evolution of σ_x at different crack lengths.

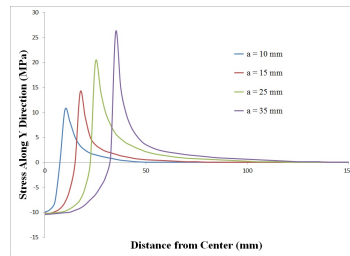


Figure 9. Evolution of σ_y at different crack lengths.

9.5 Calculation of SIF of thermal load by XIGA method

The study of convergence and comparison of the values for SIF based on the XIGA method, FEM method and the exact solution [21] are shown in Table 6 and Figure 10. In this figure, the exact solution is equal to 1.8421. The accuracy of all results is excellent, there is less than 2 percent variation in all configurations tested in the convergence range.

The calculation of the stress intensity factor in the present problem for different crack lengths is solved by the XIGA method and finite element methods, and the results are compared with those obtained from the exact solution. The results and comparisons are presented in Figure 11. The Bézier XIGA analysis is done for 2025 elements and the finite element analysis is performed for 42475 elements.

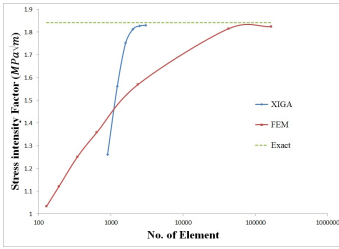


Figure 10. Study of convergence and comparison of SIF.

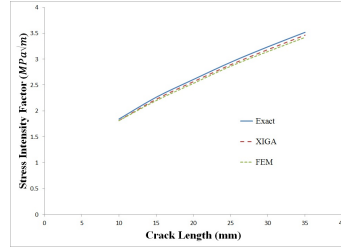


Figure 11. Comparison of SIF at different crack lengths.

Table 6. Stress intensity factor (K_1), $(pa\sqrt{m}) \times 10^7$.

No of elem.	FEM		Bézier XIGA ($p = q = 1$)		Bézier XIGA ($p = q = 2$)		Bézier XIGA ($p = q = 3$)				
	K	Error	No of elem.	K	Error	No of elem.	K	Error			
129	1.0333	%43.91	1600	1.6217	%12.0	1225	1.6527	%10.4	900	1.6578	%10.0
191	1.1203	%39.18	2025	1.7507	%4.96	1600	1.7174	%7.66	1225	1.6927	%8.01
344	1.2504	%32.12	3600	1.8071	%1.91	2500	1.7649	%4.28	1600	1.7521	%4.89
639	1.3582	%26.27	4900	1.8152	%1.46	3600	1.8101	%1.59	2025	1.8134	%1.56
2356	1.5686	%14.85	10000	1.8234	%1.02	4900	1.8193	%1.14	2500	1.8276	%0.79
42474	1.8123	%1.61	16900	1.8279	%0.77	6400	1.8252	%0.92	3025	1.8304	%0.64
166216	1.8241	%0.98	22500	1.8294	%0.68	8100	1.8289	%0.71	3600	1.8309	%0.63

9.6 Using effective SIF (K_{eff}) in crack propagation rate

Table 7 shows how K_{ther} , K_{res} and K_{eff} changes during the crack propagation. The effects of residual stress on SIF and the crack propagation rate are calculated by the modified Walker method according to Equation (8.1). The results showed that in a specified crack length, the welding residual stress considerably increases the SIF.

9.7 Fatigue crack propagation

Now, the fatigue life of a welded plate with an edge cracked is evaluated by the proposed method. The thermal load, boundary conditions, welding condition and control net are kept the same.

The material constant numbers that used in the walker equation are $c = 6 \times 10^{-12} \frac{\text{mm}}{\text{cycle}} (\text{MPa}\sqrt{m})^{-m}$, $m = 3.067$ and $\mu = 0.5$ [39]. In this study, the initial crack length is considered to be 10 mm and the crack length increment coefficient for each iteration is $c = 1.1(a_n = a_{n-1} + (0.1 \times a_0))$ until reaching the critical stress intensity factor. For SUS304 plate $K_{IC} = 219(\text{MPa}\sqrt{m})$. As shown in the above figures, the stress intensity factor is converged in the extended IGA method for a uniform control net with 2025 elements. Therefore, the domain is discretized with this control net. This problem is also solved by the finite element method using uniform quadrilateral mesh with 42475

Table 7. Result of k_{eff} and crack propagation rate

$a(mm)$	$k_{res}(MPa\sqrt{m})$	$k_{ther}(MPa\sqrt{m})$	$k_{eff}(MPa\sqrt{m})$	$\frac{da}{dN} \left(\frac{m}{cycle} \times 10^{-6} \right)$
10	39.54	1.81	41.35	1.4111
12.5	42.42	2.03	44.45	1.3026
15	44.17	2.22	46.39	1.5316
17.5	44.89	2.24	47.13	1.7059
20	44.69	2.57	47.26	1.9183
22.5	43.67	2.74	46.41	2.0927
25	41.92	2.89	44.81	2.0942
27.5	39.55	3.04	42.59	1.6493
30	36.66	3.18	39.84	1.3984
32.5	33.38	3.32	36.70	1.1526
35	29.76	3.46	33.22	0.7896
37.5	25.31	3.67	28.98	0.5604
40	20.63	3.86	24.49	0.3824

elements. A comparison of crack propagation rate obtained by the XIGA and finite element methods is shown in Figure 12. The crack growth paths obtained by both methods are almost a straight path.

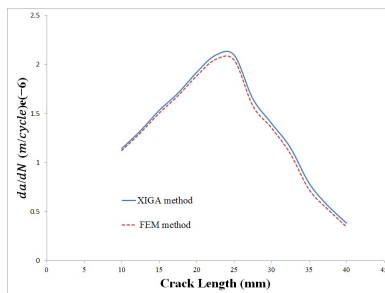


Figure 12. Fatigue life variation at different crack lengths

10 Conclusions

In this study, an extended isogeometric numerical analysis based on Bézier extraction of NURBS is developed to analyze the temperature distributions due to welding, the welding residual stress fields, the crack propagation rate and the fatigue life for the cracked plate under thermal load based on the thermo elastic-plastic equation and minimum potential energy principle. Also, the application of asymptotic enrichment functions was investigated to compute the SIF during crack growth. By comparing the obtained results, it has been proved that the presented method is an effective method for predicting these quantities. The following results are obtained:

Using the Bézier extraction operator eliminates the parametric space in the isogeometric method and mapping is done directly from the parent element to

the physical space. This will reduce the computational cost despite increasing the control points in the Bézier decomposition process. Also, the parent element used in this method, like the isoparametric element, is very similar to the element used in the Gauss quadrature integration method, which increases the accuracy of the results.

Due to the possibility of defining basic functions in each element instead of a knot span, the presented approach is more effective and accurate to analyze problems with discontinuities. This feature allows the enrichment functions correctly and only add to the basis function corresponding to the enriched element identified by level set technique

The IGA method is used to develop the thermo elastic-plastic equation, the minimum potential energy principle and the enrichment function to calculate the welding residual stress in the cracked plate. The obtained result showed an increase in accuracy and a decrease in computational cost.

Using the proposed approach, the effective SIF evaluated with acceptable accuracy and correctness by considering the concurrent effects of residual stress and thermal loading by the superposition principle, without the need for a re-meshing process around the crack.

The obtained result shows the accuracy of the modified Walker method for calculating SIF to predict crack propagation rate.

Acknowledgements

The authors reserve their utmost gratitude for advanced computing center of Islamic Azad University, Ahvaz Branch for their collaborate and technical support.

References

- [1] Standard test method for determining residual stresses by the hole- drilling strain-gage method. ASTM E837 standard-13a, 2013. <https://doi.org/10.1520/E0837-20>.
- [2] D.J. Benson, Y. Bazilevs, M.-C. Hsu and T.J.R. Hughes. A large deformation, rotation-free, isogeometric shell. *Computer Methods in Applied Mechanics and Engineering*, **200**(13):1367–1378, 2011. <https://doi.org/10.1016/j.cma.2010.12.003>.
- [3] G. Bhardwaj, I.V. Singh and B.K. Mishra. Fatigue crack growth in functionally graded material using homogenized XIGA. *Composite Structures*, **134**:269–284, 2015. <https://doi.org/10.1016/j.compstruct.2015.08.065>.
- [4] D. Bremberg and J. Faleskog. A numerical procedure for interaction integrals developed for curved cracks of general shape in 3-D. *International Journal of Solids and Structures*, **62**:144–157, 2015. <https://doi.org/10.1016/j.ijsolstr.2015.02.022>.
- [5] B. Brickstad and B.L. Josefson. A parametric study of residual stresses in multi-pass butt-welded stainless steel pipes. *International Journal of pressure Vessels and piping*, **75**(1):11–25,1998. [https://doi.org/10.1016/S0308-0161\(97\)00117-8](https://doi.org/10.1016/S0308-0161(97)00117-8).

- [6] R. Cimrman, M. Novák, R. Kolman, M. Tuma, J. Plešek and J. Vackář. Convergence study of isogeometric analysis based on bézier extraction in electronic structure calculations. *Applied Mathematics and Computation*, **319**:138–152, 2018. <https://doi.org/10.1016/j.amc.2017.02.023>.
- [7] A. de Klerk, A.G. Visser and A.A. Groenwold. Lower and upper bound estimation of isotropic and orthotropic fracture mechanics problems using elements with rotational degrees of freedom. *Communications in Numerical Methods in Engineering*, **24**(5):335–353, 2008. <https://doi.org/10.1002/cnm.973>.
- [8] H. Dehestani, Y. Ordokhani and M. Razzaghi. Numerical solution of variable-order time fractional weakly singular partial integro-differential equations with error estimation. *Mathematical Modelling and Analysis*, **25**(4):680–701, 2020. <https://doi.org/10.3846/mma.2020.11692>.
- [9] D. Deng and H. Murakawa. Numerical simulation of temperature field and residual stress in multi-pass welds in stainless steel pipe and comparison with experimental measurements. *Computational materials science*, **37**(3):269–277, 2006. <https://doi.org/10.1016/j.commatsci.2005.07.007>.
- [10] G. Glinka. Effect of residual stresses on fatigue crack growth in steel weldments under constant and variable amplitude loads. In *Fracture Mechanics: Proceedings of the Eleventh National Symposium on Fracture Mechanics: Part I*. ASTM International, 1979. <https://doi.org/10.1520/STP34914S>.
- [11] J. Huang, N. Nguyen-Thanh, W. Li and K. Zhou. An adaptive isogeometric-meshfree coupling approach for the limit analysis of cracked structures. *Theoretical and Applied Fracture Mechanics*, **106**:102426, 2020. <https://doi.org/10.1016/j.tafmec.2019.102426>.
- [12] X. Huang, Y. Liu and X. Huang. Analytical characterizations of crack tip plastic zone size for central-cracked unstiffened and stiffened plates under biaxial loading. *Engineering Fracture Mechanics*, **206**:1–20, 2019. <https://doi.org/10.1016/j.engfracmech.2018.11.047>.
- [13] T.J.R. Hughes, J.A. Cottrell and Y. Bazilevs. Isogeometric analysis: CAD, finite elements, NURBS, exact geometry and mesh refinement. *Computer methods in applied mechanics and engineering*, **194**(39):4135–4195, 2005. <https://doi.org/10.1016/j.cma.2004.10.008>.
- [14] A. Jameel and G.A. Harmain. A coupled FE-IGA technique for modeling fatigue crack growth in engineering materials. *Mechanics of Advanced Materials and Structures*, **26**(21):1764–1775, 2019. <https://doi.org/10.1080/15376494.2018.1446571>.
- [15] A. Jameel and G.A. Harmain. Extended iso-geometric analysis for modeling three-dimensional cracks. *Mechanics of Advanced Materials and Structures*, **26**(11):915–923, 2019. <https://doi.org/10.1080/15376494.2018.1430275>.
- [16] A. Jameel and G.A. Harmain. Fatigue crack growth analysis of cracked specimens by the coupled finite element-element free Galerkin method. *Mechanics of Advanced Materials and Structures*, **26**(16):1343–1356, 2019. <https://doi.org/10.1080/15376494.2018.1432800>.
- [17] A. Jameel and G.A. Harmain. Large deformation in bi-material components by XIGA and coupled FE-IGA techniques. *Mechanics of Advanced Materials and Structures*, **29**(6):850–872, 2022. <https://doi.org/10.1080/15376494.2020.1799120>.

- [18] B. Karaman. On the numerical simulation of time-space fractional coupled nonlinear schrödinger equations utilizing wendland's compactly supported function collocation method. *Mathematical Modelling and Analysis*, **26**(1):94–115, 2021. <https://doi.org/10.3846/mma.2021.12262>.
- [19] M. Kern, A. Taakili and M.M. Zarrouk. Preconditioned iterative method for reactive transport with sorption in porous media. *Mathematical Modelling and Analysis*, **25**(4):546–568, 2020. <https://doi.org/10.3846/mma.2020.10626>.
- [20] W. Li, N. Nguyen-Thanh, J. Huang and K. Zhou. Adaptive analysis of crack propagation in thin-shell structures via an isogeometric-meshfree moving least-squares approach. *Computer Methods in Applied Mechanics and Engineering*, **358**:112613, 2020. <https://doi.org/10.1016/j.cma.2019.112613>.
- [21] A.M. Malik, E.M. Qureshi, N.U. Dar and I. Khan. Analysis of circumferentially arc welded thin-walled cylinders to investigate the residual stress fields. *Thin-Walled Structures*, **46**(12):1391–1401, 2008. <https://doi.org/10.1016/j.tws.2008.03.011>.
- [22] A. Moarrefzadeh, S. Shahrooi and M.J. Azizpour. Predicting fatigue crack propagation in residual stress field due to welding by meshless local Petrov-Galerkin method. *Journal of Manufacturing Processes*, **45**:379–391, 2019. <https://doi.org/10.1016/j.jmappro.2019.07.019>.
- [23] S. Murugan, S.K. Rai, P.V. Kumar, T. Jayakumar, B. Raj and M.S.C Bose. Temperature distribution and residual stresses due to multipass welding in type 304 stainless steel and low carbon steel weld pads. *International Journal of Pressure vessels and piping*, **78**(4):307–317, 2001. [https://doi.org/10.1016/S0308-0161\(01\)00047-3](https://doi.org/10.1016/S0308-0161(01)00047-3).
- [24] L.B. Nguyen, C.H. Thai, A.M. Zenkour and H. Nguyen-Xuan. An isogeometric Bézier finite element method for vibration analysis of functionally graded piezoelectric material porous plates. *International Journal of Mechanical Sciences*, **157–158**:165–183, 2019. <https://doi.org/10.1016/j.ijmecsci.2019.04.017>.
- [25] N. Nguyen-Thanh, J. Huang and K. Zhou. An isogeometric-meshfree coupling approach for analysis of cracks. *International Journal for Numerical Methods in Engineering*, **113**(10):1630–1651, 2018. <https://doi.org/10.1002/nme.5713>.
- [26] N. Nguyen-Thanh, N. Valizadeh, M.N. Nguyen, H. Nguyen-Xuan, X. Zhuang, P. Areias, G. Zi, Y. Bazilevs, L. De Lorenzis and T. Rabczuk. An extended isogeometric thin shell analysis based on Kirchhoff–Love theory. *Computer Methods in Applied Mechanics and Engineering*, **284**:265–291, 2015. <https://doi.org/10.1016/j.cma.2014.08.025>.
- [27] L. Piegl and W. Tiller. *The NURBS book*. Springer Science & Business Media, 2012. <https://doi.org/10.1007/978-3-642-97385-7>.
- [28] M. Ratas, A. Salupere and J. Majak. Solving nonlinear PDEs using the higher order Haar wavelet method on nonuniform and adaptive grids. *Mathematical Modelling and Analysis*, **26**(1):147–169, 2021. <https://doi.org/10.3846/mma.2021.12920>.
- [29] A.H.S. Shayegan, A. Zakeri and S.M. Hosseini. A numerical method for solving two-dimensional nonlinear parabolic problems based on a preconditioning operator. *Mathematical Modelling and Analysis*, **25**(4):531–545, 2020. <https://doi.org/10.3846/mma.2020.4310>.
- [30] J. Shi, D. Chopp, J. Lua, N. Sukumar and T. Belytschko. Abaqus implementation of extended finite element method using a level set

- representation for three-dimensional fatigue crack growth and life predictions. *Engineering Fracture Mechanics*, **77**(14):2840–2863, 2010. <https://doi.org/10.1016/j.engfracmech.2010.06.009>.
- [31] A.K. Singh, A. Jameel and G.A. Harmain. Investigations on crack tip plastic zones by the extended iso-geometric analysis. *Materials Today: Proceedings*, **5**(9):19284–19293, 2018. <https://doi.org/10.1016/j.matpr.2018.06.287>.
- [32] J. Sladek, P. Stanak, Z.D. Han, V. Sladek and S.N. Atluri. Applications of the MLPG method in engineering & sciences: a review. *CMES: Computer Modeling in Engineering & Sciences*, **92**(5):423–475, 2013.
- [33] M. Španiel, J. Jurenka and J. Kuželka. Verification of FE model of fatigue crack propagation under mixed mode conditions. *Meccanica*, **44**(2):189–195, 2009. <https://doi.org/10.1007/s11012-008-9164-0>.
- [34] G.F. Sun, Z.D. Wang, Y. Lu, R. Zhou, Z.H. Ni, X. Gu and Z.G. Wang. Numerical and experimental investigation of thermal field and residual stress in laser-mig hybrid welded NV E690 steel plates. *Journal of Manufacturing Processes*, **34**:106–120, 2018. <https://doi.org/10.1016/j.jmapro.2018.05.023>.
- [35] A. Sutradhar and G.H. Paulino. Symmetric Galerkin boundary element computation of T-stress and stress intensity factors for mixed-mode cracks by the interaction integral method. *Engineering Analysis with Boundary Elements*, **28**(11):1335–1350, 2004. <https://doi.org/10.1016/j.enganabound.2004.02.009>.
- [36] L.V. Tran, A.J.M. Ferreira and H. Nguyen-Xuan. Isogeometric analysis of functionally graded plates using higher-order shear deformation theory. *Composites Part B: Engineering*, **51**:368–383, 2013. <https://doi.org/10.1016/j.compositesb.2013.02.045>.
- [37] R. Vaghefi, M.R. Hematiyan, A. Nayebi and A. Khosravifard. A parametric study of the MLPG method for thermo-mechanical solidification analysis. *Engineering Analysis with Boundary Elements*, **89**:10–24, 2018. <https://doi.org/10.1016/j.enganabound.2018.01.006>.
- [38] W. Wen, S. Luo, S. Duan, J. Liang and D. Fang. Improved quadratic isogeometric element simulation of one-dimensional elastic wave propagation with central difference method. *Applied Mathematics and Mechanics*, **39**(5):703–716, 2018. <https://doi.org/10.1007/s10483-018-2330-6>.
- [39] B. Yahiaoui and P. Petrequin. Étude de la propagation de fissures par fatigue dans des aciers inoxydables austénitiques à bas carbone du type 304l et 316l. *Revue de Physique Appliquée*, **9**(4):683–690, 1974. <https://doi.org/10.1051/rphysap:0197400904068300>.
- [40] S. Yin, T. Yu, T.Q. Bui, X. Zheng and S. Gu. Static and dynamic fracture analysis in elastic solids using a multiscale extended isogeometric analysis. *Engineering Fracture Mechanics*, **207**:109–130, 2019. <https://doi.org/10.1016/j.engfracmech.2018.12.024>.
- [41] H. Yuan, W.J. Liu and Y.J. Xie. Mode-I stress intensity factors for cracked special-shaped shells under bending. *Engineering Fracture Mechanics*, **207**:131–148, 2019. <https://doi.org/10.1016/j.engfracmech.2018.12.026>.
- [42] M. Zubairuddin, S.K. Albert, M. Vasudevan, S. Mahadevan, V. Chaudhari and V.K. Suri. Numerical simulation of multi-pass GTA welding of grade 91 steel. *Journal of Manufacturing Processes*, **27**:87–97, 2017. <https://doi.org/10.1016/j.jmapro.2017.04.031>.